

50-2731  
Copy 84

RM A9I29

NACA RM A9I29

A9I 29

TIE3

NACA

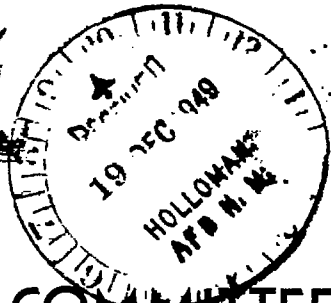


# RESEARCH MEMORANDUM

EXPERIMENTAL INVESTIGATION AT SUPERSONIC SPEEDS OF  
SIDE SCOOPS EMPLOYING BOUNDARY-LAYER SUCTION

By Sherman S. Edwards

Ames Aeronautical Laboratory  
Moffett Field, Calif.



NATIONAL ADVISORY COMMITTEE  
FOR AERONAUTICS

WASHINGTON  
December 12, 1949

215 F 105



0142958

NACA RM A9I29

## NATIONAL ADVISORY COMMITTEE FOR AERONAUTICS

RESEARCH MEMORANDUMEXPERIMENTAL INVESTIGATION AT SUPERSONIC SPEEDS OF  
SIDE SCOOPS EMPLOYING BOUNDARY-LAYER SUCTION

By Sherman S. Edwards

## SUMMARY

The pressure-recovery characteristics of a model having two scoops situated on the aft portion of a long forebody and connected through diffusers to a common settling chamber were determined at Mach numbers between 1.36 and 2.01 and Reynolds numbers (based upon the length of the model ahead of the inlets) between 2.6 and 3.4 million. The boundary layer present on the forebody of the model ahead of the main scoops was removed by means of boundary-layer suction scoops. Total pressure and mass flow in the main and boundary-layer ducts were measured in tests in which the approach to the inlets and the model angle of attack were varied. The effects of interaction between the flow in the two air-induction systems and of varying the mass flow through the boundary-layer scoops were studied.

At Mach numbers less than 1.8, it was found that, by properly designing the approach to the inlets and neglecting the energy expended in boundary-layer removal, total-pressure recovery within 0.05 of that of nose inlets could be maintained over a large range of mass-flow ratios. By full-scale extrapolation of the data, it was estimated that the energy required for removal of the boundary layer was equivalent to a loss in total pressure of approximately 0.04 of the measured recovery in the main scoops. The total-pressure ratio was found to decrease with increasing positive angles of attack. An improvement in the pressure recovery occurred at angle of attack when the forebody was drooped with respect to the duct inlets.

## INTRODUCTION

In reference 1 it was found that the total-pressure recovery obtained with scoop inlets compared favorably with that obtained with nose inlets over a relatively large range of mass-flow ratio and up to free-stream Mach numbers of about 1.70. The results indicated that improved pressure recovery depended primarily upon boundary-layer-control measures designed both to remove low-energy air from the ducts and to prevent premature separation of the boundary layer ahead of the scoops. In the models tested, the boundary layer was diverted through slots in

CONFIDENTIAL

2737

the scoop side walls immediately behind the inlet and contiguous to the model forebody. From these results, it appeared reasonable to assume that boundary-layer control by means of slots could be replaced by suction scoops and that equally high pressure recovery would result. The latter method of removing the boundary layer possibly would have advantages of arrangement, reduced external drag, and reduced effects of boundary-layer shock-wave interaction ahead of the inlets.

It is the purpose of the present report to describe tests of a specific configuration which employed boundary-layer control by means of suction scoops and to investigate modifications in the model designed to improve the maximum pressure recovery. No study was made of the external drag contributed by the inlets. In selecting an optimum inlet design, this important variable would have to be considered further.

#### SYMBOLS

A	area, square inches
H	total pressure, pounds per square foot
M	Mach number
m	rate of mass flow, pounds per second
R	Reynolds number
$\alpha$	angle of attack, degrees
$\delta$	boundary-layer thickness, inches
$\bar{H}_2/H_0$	ratio of the average total pressure at position 2 to the free-stream total pressure $\left[ \bar{H}_2/H_0 = \frac{1}{A} \sum_{n=1}^{n=5} (H_2/H_0)_n \Delta A_n \right]$ , where n refers to area divisions and tube locations
$(\bar{H}_2/H_0)_e$	equivalent total-pressure ratio at position 2, the difference between $\bar{H}_2/H_0$ and the energy expended in boundary-layer removal
$m_1/m_0$	ratio of the mass flow entering the main scoops to that which would flow through a tube of the same inlet area in the free stream
$m_4/m_0$	ratio of the mass flow entering the boundary-layer scoops to that which would flow through a tube of the same inlet area in the free stream

The following subscripts indicate the position at which the quantities were measured (fig. 1):

- 0 free stream
- 1 entrance to main scoop
- 2 survey position immediately downstream of main-scoop entrance
- 3 settling chamber
- 4 entrance to boundary-layer scoops
- 5 survey station in boundary-layer removal duct

#### APPARATUS AND MODELS

The tests were performed in the Ames 8- by 8-inch supersonic wind tunnel at Mach numbers between 1.36 and 2.01 and Reynolds numbers, based upon the length of the model ahead of the inlets (3.934 in.), of 2.6 to 3.4 million. Flow through the boundary-layer removal ducts was exhausted to the atmosphere through a vacuum pump. A description of the equipment and wind tunnel can be found in references 2 and 3.

The model (see figs. 1 and 2) was built to simulate the forward portion of the fuselage and the ducts of a possible supersonic airplane designed to fly in the speed range up to a Mach number of 2.0. In designing the scoops two variables were compromised: First, to supply efficiently the air consumed by engines capable of driving the airplane at these speeds, large inlet areas would be required below a Mach number of about 0.5, and small areas would be required in the supersonic range; and, second, large leading-edge radii would be desirable to prevent the flow from stalling on the inside surface of the lips at subsonic speeds, and sharp leading edges would be desirable to decrease the wave drag at supersonic speeds. These situations were compromised by choosing the inlet area large enough so that a normal shock wave would form ahead of the inlet at all supersonic speeds. Thus, by choosing the inlet areas sufficiently large, auxiliary inlets would be unnecessary in the subsonic range. Furthermore, large leading-edge radii would be permissible since the flow behind the normal shock wave always would be subsonic. At supersonic speeds, the large inlet area would result in spilling of the air around the inlets at the expense, of course, of increased external drag.

Conical subsonic diffusors commonly used at low speeds have a severe adverse pressure gradient near their entrance when operated at high inlet Mach numbers. It was assumed that decreasing this gradient would reduce the tendency toward separation of the boundary layer; hence the internal shape of the main ducts was designed to have a constant static-pressure gradient from the inlet to a station approximately 20 percent of the

diffusor length aft of the inlet. Downstream of this point the cross-sectional areas of each duct were adjusted to arrive at the cross section of the common settling chamber.

The model dimensions are given in figure 1, and a photograph of the model tested is shown in figure 2. The model forebody was roughly triangular in cross section, and the scoops were located aft of the pilot enclosure in a position to utilize the oblique shock waves originating from the enclosure for external compression of the air stream. Aft of the main inlets, the external shape of the model was faired to adapt it to a cylindrical settling chamber.

The original design, hereafter designated configuration A, and five modifications to this design were tested. In configurations B, C, and D the model contours in the critical region near the entrance to the scoops were modified as shown in the line drawings of figure 3. In configurations E and F, the contours in the vicinity of the inlet were identical to those of configuration D; however, the model forebody was drooped with respect to the duct inlets. As noted in figure 1, the model with the forebody incidence reduced  $2^\circ$  is designated configuration E and that reduced  $6^\circ$  is configuration F.

#### TESTS

In general, an analysis of the performance of the duct inlet design tested is concerned with a study of the following six variables: total-pressure recovery, free-stream Mach number, mass flow through the main scoops, mass flow through the boundary-layer scoops, angle of attack, and the inlet's contribution to the external drag. In the present tests the last variable was neglected, and the total-pressure recovery was chosen as the dependent variable. Thus, the performance of the model was studied by investigating the total-pressure recovery as a function of the remaining four variables.

Variation in the mass flow into the main scoops was obtained by changing the position of the plug at the rear of the settling chamber (fig. 1). The total-pressure ratio across the exit plug was sufficient to maintain a sonic throat at the minimum area at all times. This fact, together with the known stagnation temperature and measurements of the average total pressure in the settling chamber, allowed the rate of mass flow through the scoops to be calculated (reference 1).

Variation in the flow into the boundary-layer scoops was obtained by means of a valve in the line leading to the vacuum pump. The total pressure recovered in the boundary-layer scoops was measured by a pitot tube located at position 5 as shown in figure 1. The rate of mass flow through the boundary-layer scoops was determined by measuring the total pressure at the center and static pressure at the wall of a  $3/4$ -inch pipe located outside the tunnel and by assuming a velocity profile corresponding to that for fully developed turbulent flow. Because it was

impossible to simulate full-scale ducting in the suction system with a model of this scale, more precise measurements of these quantities were not made. These data are probably most valuable for their qualitative significance.

Measurements of the total pressure in the settling chamber were made at three equally spaced circumferential locations at the position indicated in figure 1. The area ratio between the total scoop-entrance area and the cross-sectional area of the settling chamber was 0.07 which, for isentropic diffusion from sonic velocity, would correspond to a settling-chamber Mach number of about 0.04. With this degree of diffusion, it was considered unnecessary to attempt a further survey of the total pressure other than that afforded by the three pitot tubes. This assumption was substantiated by the fact that the difference in total pressure measured by each of the three tubes was within 2 percent of the average of those tubes at every rate of mass flow.

In order to determine the effect of the subsonic diffusors upon the values of total pressure measured in the settling chamber of the model, the total-pressure distribution at position 2 was obtained. The average computed Mach number at this position was approximately 0.50 at mass-flow ratios at which the normal shock wave was ahead of the inlets. Measurements of the total pressure were made in both ducts with the model at an angle of attack of  $0^{\circ}$ . The measurement locations are shown in figure 4. As indicated in the figure, each location was numbered and the duct cross section at this position was divided to obtain a weighted average of the total-pressure measurements. Properly weighted values of  $H_2/H_0$  would have been based upon the mass flow through the area divisions shown in figure 4. Since measurements of these mass flows were impossible because of the model scale, the weighted averages were based upon the areas.

#### RESULTS AND DISCUSSION

The results will be discussed in two parts. In the first section, test results at an angle of attack of  $0^{\circ}$  are discussed. In this section, model modifications designed to improve the pressure recovery throughout the Mach number range are investigated, and the effects of variations in the parameters  $m_1/m_0$  and  $m_4/m_0$  upon the total-pressure recovery of the best configuration are discussed. Also, in this section, the performance of the best model is analyzed with respect to the total-pressure distribution within the ducts, interaction between duct systems, and estimated energy expended in boundary-layer removal. Finally, in the second section, the effects of variations in angle of attack are treated, and modifications designed to improve the pressure recovery at angle of attack are discussed.

~~CONFIDENTIAL~~

## Angle of Attack of 0°

Effect of Mach number on pressure recovery.— Maximum total-pressure ratios  $(H_s/H_0)_{\max}$  as a function of the free-stream Mach number are presented in figure 5 for the four inlet configurations, A, B, C, and D, that were tested at an angle of attack of 0°. From an examination of the curves in this figure, it is apparent that the changes in the inlet, shown in figure 3, improved the pressure recovery. Examination of schlieren photographs of the flow about inlet configuration A indicated that an expansion region originating at the leading edge of the boundary-layer scoop extended into the flow immediately ahead of the main inlet. This expansion was caused by improper alignment of the outer surface of the boundary-layer lip with the flow on the pilot enclosure. In order to eliminate this expansion in configuration B, the lip of the boundary-layer scoop was shaped to form a 5° angle with the surface of the cockpit enclosure, and the height of the boundary-layer scoop was increased to insure complete removal of the boundary layer. With this modification, the expansion ahead of the main scoop was replaced by an oblique shock wave and a greater pressure recovery resulted. By further increasing the angle formed by the outer surface of the boundary-layer scoop and the cockpit enclosure in configuration C, this oblique shock wave was strengthened and the total-pressure recovery was improved. However, the pressure recovery at the highest Mach number tested was still the same as that of configuration B. The decrease in pressure recovery at  $M_\infty$  equal to 2.01 apparently was caused by the fact that the intersection of the stronger oblique shock wave and the normal shock wave was inboard of the lip of the scoop. Thus, the air that entered the scoop near the outer lip suffered larger losses in total pressure through a strong normal shock wave than was experienced by the air that passed through both an oblique and normal shock wave.

Highest total-pressure recovery was obtained with configuration D. In figure 3 this configuration is shown to be similar to C, except that the leading edge of the boundary-layer scoop was extended farther ahead of the main inlet. The purpose of this modification was to retain the oblique shock strength of configuration C and to enable the oblique shock wave to extend across the inlet at a Mach number of 2.0. Schlieren photographs and line drawings of the shock-wave patterns ahead of the inlets of this configuration are shown in figure 6. At a free-stream Mach number of 2.0 the oblique shock wave from the leading edge of the boundary-layer scoop is shown to intersect the normal shock wave at a point slightly outboard of the scoop. Thus, all the air that entered the inlets underwent compression through the oblique shock wave before encountering the normal shock wave.

Since the flow in the settling chamber of the model was diffused to a Mach number much lower than the usual intake Mach number at the compressor of a turbojet engine, the measured values of  $(H_s/H_0)_{\max}$  include diffusion losses that would not occur in an airplane.

~~CONFIDENTIAL~~

The total-pressure surveys at position 2 were made in a section of the duct where the computed average Mach number was approximately 0.5, and these measurements represent more closely the pressure recovery that would exist at the compressor intake. The variation of  $(\bar{H}_2/H_0)_{max}$  with  $M_0$  for configuration D is shown in figure 5. The losses in total-pressure ratio between positions 2 and 3 amounted to from 0.015 to 0.030.

Since the nose-type duct inlet is generally accepted, at present, as a design in which the highest pressure recovery can be realized, the pressure recovery of typical nose inlet models (reference 4) is also shown in figure 5. A comparison of these results with those of the present model indicates that, at Mach numbers less than about 1.8, total-pressure recovery within 0.05 of that of nose inlets was attained with the present design, without considering energy expended in removing boundary-layer air.

Effect of mass-flow ratio  $m_1/m_0$  on pressure recovery.— The variation of  $H_5/H_0$  and  $\bar{H}_2/H_0$  with  $m_1/m_0$  is presented in figure 7 for configuration D at an angle of attack of  $0^\circ$ . In the range of mass-flow ratios indicated by the dashed curves, schlieren photographs demonstrated that the boundary layer ahead of the scoops was separated. The fact that the total-pressure ratio  $H_5/H_0$  remained high at 1.36 Mach number possibly was caused by a condition in which the losses ahead of the inlet were compensated for by reduced losses within the subsonic diffusors at these low mass-flow ratios. Apparently, as the Mach number increased the energy dissipated in turbulence ahead of the inlet increased and caused reduced values of  $H_5/H_0$  noted at the higher Mach numbers.

Maximum values of  $\bar{H}_2/H_0$  occurred at larger mass-flow ratios than those at which  $(H_5/H_0)_{max}$  was recorded. This difference can be attributed to the subsonic diffusor efficiency between the two positions. The attainment of a constant rate of mass flow through the air-induction system indicates that supersonic flow into the inlet has been established.

Effect of mass-flow ratio  $m_4/m_0$  on pressure recovery.— The previously discussed results were obtained with the maximum rate of flow through the boundary-layer scoops. In tests of the model with inlet configuration D, reductions in the mass of air flowing through the boundary-layer scoops influenced the recovery of total pressure in the settling chamber as shown in figure 8. A nearly linear variation of  $(H_5/H_0)_{max}$  with  $m_4/m_0$  occurred at free-stream Mach numbers of 1.36 and 1.70. However, for  $M_0$  equal to 2.01, a reduction in  $m_4/m_0$  from the value at which the flow in the boundary-layer duct was choked caused the main-scoop flow to be unsteady and  $H_5/H_0$  to decrease markedly.

For configuration D with choked flow in the boundary-layer ducts, the mass-flow ratio  $m_4/m_0$  of the air entering the boundary-layer scoops and the total-pressure recovery  $H_5/H_0$  in the sting are presented in figure 9 as functions of  $m_1/m_0$ . At mass-flow ratios at which separated flow occurred ahead of the main scoops (see fig. 7), the reduced pressure

recovery and mass flow in the boundary-layer scoops indicate that the boundary layer separated ahead of the boundary-layer scoops as well. In the tests with the maximum rate of flow through the boundary-layer ducts, the pressure in the sting  $H_5$  was maintained at the highest value at which no adverse influence on the main duct system was noted. The relatively low values of  $H_5/H_0$  can be attributed to pressure losses in the boundary-layer ducts in addition to the energy dissipated in the boundary layer along the model forebody.

Total-pressure distribution in duct.— The survey of the total pressure within the duct at position 2 affords a means of estimating the asymmetry in the total pressure of the air flow that would be supplied to a compressor. This factor is important when considering compressor performance or the repeated stresses likely to be imposed upon the compressor blades. In figure 10, the pressure distribution across the height and width of one duct is shown for three values of  $m_1/m_0$  and Mach number. The occurrence of greater asymmetry in the pressure distribution as the free-stream Mach number was increased possibly was caused by the greater intensity of the effects of boundary-layer shock-wave interaction which would result in thickening or separation of the boundary layer. Total pressures near the floor of the duct were consistently low at all Mach numbers and mass-flow ratios indicating that, in the presence of the adverse pressure gradient at the entrance to the scoops, the boundary layer thickens rapidly from the leading edge of the boundary-layer scoop. The maximum variation in total-pressure ratio occurred at a Mach number of 2.01, in which case the difference between the maximum and minimum pressure recovery was approximately 40 percent of the average total-pressure recovery at position 2. This variation is large, but at full scale a smaller variation could be expected because of the much greater Reynolds number and reduced viscous effects.

Interaction between duct systems.— An interaction between the flows in the two main diffusors was manifest in measurements of the total pressure at position 2. With decreasing values of  $m_1/m_0$  from that at which separated flow occurred ahead of the inlets, the pressure recovery at this position in the two ducts diverged about an average value approximately equal to  $H_3/H_0$ . It was impossible to predict the particular duct passage in which the pressure recovery would diverge above or below the average; however, once the recovery in one side of the induction system had been established above the average, it continued to diverge in this direction with decreasing values of  $m_1/m_0$ . This result indicated a possible reversal of flow in one duct at this condition.

To observe the effects upon the pressure recovery and flow stability of single-duct operation, tests were performed with one duct sealed. The boundary layer was removed ahead of the closed duct in order to reduce the possibility that this flow would influence the flow in the open duct. Results of these tests indicated that separation occurred at about 10-percent-lower values of  $m_1/m_0$  and 2-percent-higher total-pressure ratios  $H_5/H_0$  than are shown in figure 7.

Estimate of the energy expended in boundary-layer removal.— The equivalent pressure recovery obtained by subtracting the energy required for boundary-layer removal from the measured recovery does not provide a completely adequate criterion for the worth of this system. In considering a specific application, the advantages of arrangement that may result from use of side scoops with boundary-layer control, possible uses of the boundary-layer air such as in engine cooling, and the results of a detailed analysis of the effects of the inlets upon the external drag would also have to be considered. In order to obtain an indication of the effective recovery, however, the energy expended in the boundary-layer scoops was subtracted from the energy recovered in the main scoops in order to arrive at an equivalent value of the pressure recovery at position 2,  $(\bar{H}_2/H_0)_e$ .

The tables of reference 5 were used in these calculations and the experimental results were applied to full-scale flight at an altitude of 35,000 feet. It was assumed that the energy required to remove the boundary layer was equal to that necessary to compress isentropically the mass flow in the boundary-layer scoop  $m_4$  from the total pressure after diffusion  $H_5$  to a total pressure  $H_4$  corresponding to a 50-percent decrease in the free-stream kinetic energy. The latter assumes a turbulent boundary layer at the entrance to the boundary-layer scoops and that the energy contained in the boundary layer is equal to that of the free stream depleted of 50 percent of its kinetic energy. The results of calculations making use of the preceding assumptions are shown in figure 11. Values of  $(\bar{H}_2/H_0)_e$  were calculated within the range of mass-flow ratio at which the flow into the scoops of configuration D was steady. A comparison of these results with the measured pressure recovery at position 2 indicates that the energy required to remove the boundary layer was equivalent to a loss in total pressure  $\bar{H}_2/H_0$  of approximately 0.08.

The extension of the data to full scale, however, requires some consideration of the effect of the model scale, which was taken as 1.4 percent. In estimating the influence of the model scale, the following assumptions were made:

1. The boundary layer at the entrance to the boundary-layer scoops was turbulent.
2. The boundary-layer thickness on the model and at full scale varies as

$$\frac{(\delta/x)_{\text{model}}}{(\delta/x)_{\text{full scale}}} = \left[ \frac{(R_x)_{\text{full scale}}}{(R_x)_{\text{model}}} \right]^{1/5}$$

where  $x$  is a characteristic length. (See reference 6.)

3. The mass-flow ratio  $m_4/m_0$ , required at full scale to produce the same pressure recoveries as were recorded in the model tests, was equal to

$$(m_4/m_0)_{\text{full scale}} = \frac{(m_4/m_0)_{\text{model}}}{[(R_x)_{\text{full scale}}/(R_x)_{\text{model}}]^{1/5}}$$

The results of applying these assumptions regarding the influence of the model scale to the previous calculations are also shown in figure 11. In this case the energy required to remove the boundary layer was equivalent to a decrease in the total pressure ratio  $\bar{H}_2/H_0$  of approximately 0.04.

#### Angle of Attack

Configuration D.— The variation of total-pressure recovery with mass flow is shown in figure 12 for configuration D at angle of attack. An examination of these results indicates that  $(H_s/H_0)_{\text{max}}$  decreased with increasing positive angles of attack, and that the range of mass-flow ratios in which large values of  $H_s/H_0$  could be maintained was markedly reduced. The schlieren photographs of figure 13 indicate that the thickness of the boundary layer along the forebody ahead of the scoop increased as the angle of attack of the model was increased.<sup>1</sup> Thus the boundary-layer scoops were apparently inadequate in handling this thicker boundary layer. The greater boundary-layer thickness at angle of attack may have been caused by a secondary flow in the boundary layer due to the pressure difference between the upper and lower surfaces of the forebody. The low values of the total-pressure recovery measured at position 3 probably are greatly influenced by the presence of this boundary layer in the subsonic diffusor at angle of attack. In all tests of the model at angle of attack, the mass flow in the boundary-layer scoops was maintained at the choked condition.

Forebody incidence.— To improve the pressure recovery at angle of attack the forebody was drooped  $2^\circ$  and  $6^\circ$  with respect to the inlets. (See fig. 2.) Maximum values of  $H_s/H_0$  as functions of  $M_0$  are presented in figure 14 for configurations E and F at various angles of attack. The values of  $(H_s/H_0)_{\text{max}}$  measured in tests of configuration D are also shown for purposes of comparison. Improvements in  $(H_s/H_0)_{\text{max}}$  occurred in tests of E and F; however, the total-pressure recovery at  $6^\circ$  and  $9^\circ$  angle of attack still was low when compared to that at  $0^\circ$ . In figure 14, configuration F at  $6^\circ$  angle of attack did not give the same pressure recovery as configuration D at  $0^\circ$  angle of attack due to the fact that

---

<sup>1</sup>In these photographs the model is both at an angle of attack and side-slip because it was necessary to rotate the model about its longitudinal axis in order to photograph the boundary layer on the forebody ahead of one scoop.

the models were slightly different. In configuration F, an expansion occurs at station 2.681 which probably changed the shock-wave pattern immediately ahead of the inlet.

The variation of  $H_s/H_0$  with  $m_1/m_0$  measured in tests of configurations E and F is shown in figures 15 and 16. Comparison of these results with similar curves of configuration D, shown in figures 7 and 12, indicates that, at an angle of attack of  $0^\circ$  and at a Mach number of 2.01, drooping the forebody of the model improved the range of mass-flow ratios over which  $H_s/H_0$  was maintained at relatively high values. A similar improvement, but to a lesser degree, can be noted at angle of attack.

#### CONCLUSIONS

From tests at Mach numbers between 1.36 and 2.01 and Reynolds numbers between 2.6 and 3.4 million (based upon the length of the model ahead of the inlets) of several configurations of a duct-inlet model having side scoops and employing boundary-layer suction, the following conclusions are drawn:

1. For the best configuration developed in the investigation, it was found that the arrangement advantages of side scoops can be utilized with total-pressure recovery within 0.05 of that of nose inlets neglecting the energy expended in boundary-layer removal at free-stream Mach numbers less than 1.8.
2. The total-pressure distribution within the ducts was nonuniform, and the variation increased with free-stream Mach number.
3. The energy expended in removing the boundary layer at full-scale flight conditions was estimated to be equivalent to a reduction of approximately 0.04 of the measured total-pressure recovery.
4. The total-pressure recovery decreased with increasing positive angles of attack. Drooping the forebody of the model with respect to the inlets improved the pressure recovery at angle of attack, and the range of mass-flow ratios in which high pressure recovery could be maintained was increased.

Ames Aeronautical Laboratory,  
National Advisory Committee for Aeronautics,  
Moffett Field, Calif.

## REFERENCES

1. Davis, Wallace F., Edwards, Sherman S., and Brajnikoff, George B.: Experimental Investigation at Supersonic Speeds of Twin-Scoop Duct Inlets of Equal Area. IV - Some Effects of Internal Duct Shape Upon an Inlet Enclosing 37.2 Percent of the Forebody Circumference. NACA RM A9A31, 1949.
2. Davis, Wallace F., Brajnikoff, George B., Goldstein, David L., and Spiegel, Joseph M.: An Experimental Investigation at Supersonic Speeds of Annular Duct Inlets Situated in a Region of Appreciable Boundary Layer. NACA RM A7G15, 1947.
3. Allen, H. Julian: The Asymmetric Adjustable Supersonic Nozzle for Wind-Tunnel Application. NACA RM A8E17, 1948.
4. Ferri, Antonio, and Nucci, Louis M.: Preliminary Investigation of a New Type of Supersonic Inlet. NACA RM L6J31, 1946.
5. Keenan, Joseph H., and Kaye, Joseph: A Table of Thermodynamic Properties of Air. Jour. App. Mech., vol. 10, no. 3, Sept. 1943, pp. A-123-A130.
6. Durand, W. F.: Aerodynamic Theory, vol. III, The Mechanics of Viscous Fluids, sec. 23, J. Springer (Berlin), 1934, pp. 145-154.

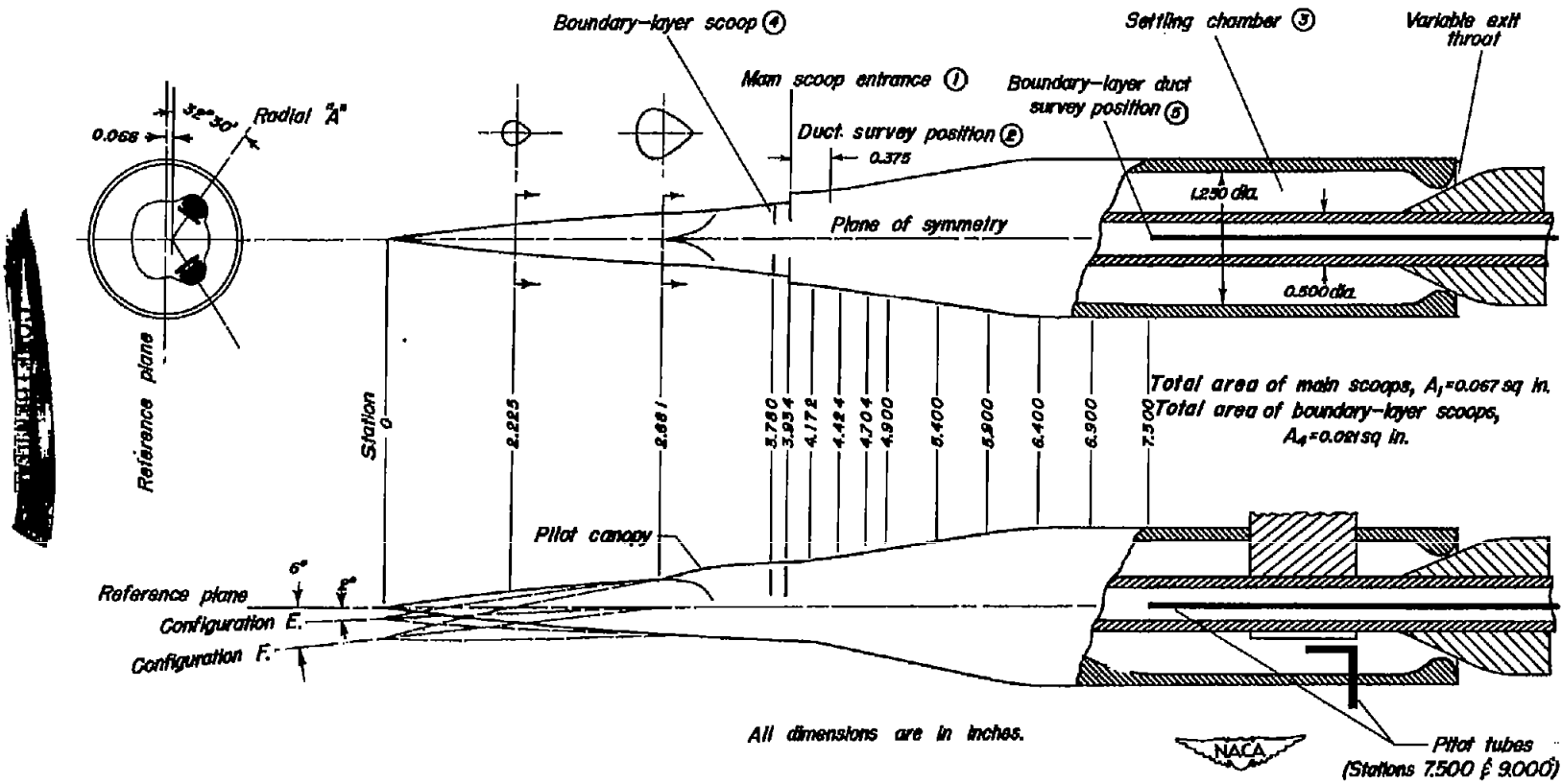
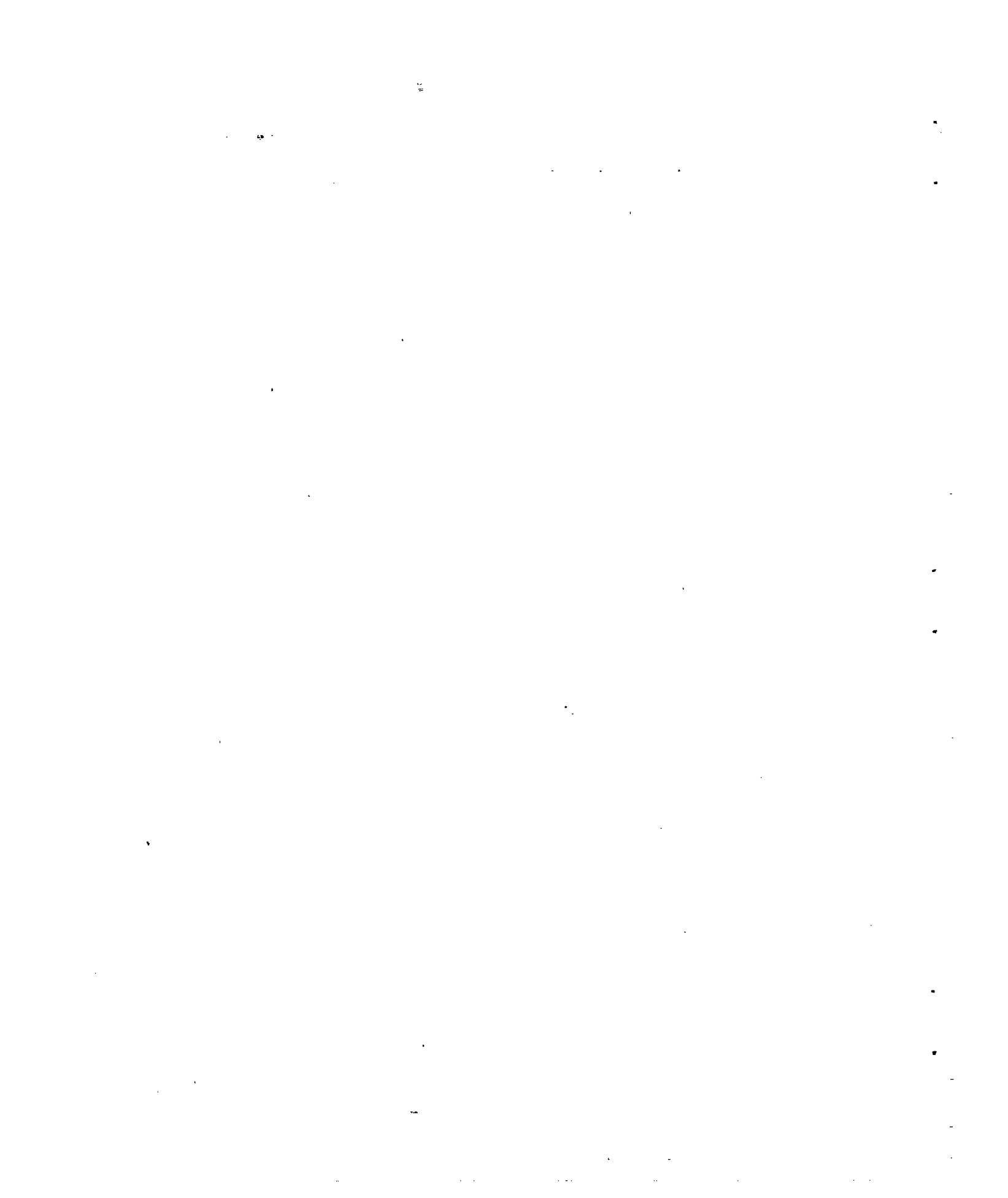


Figure 1.— Model dimensions.



NACA RM A9T29

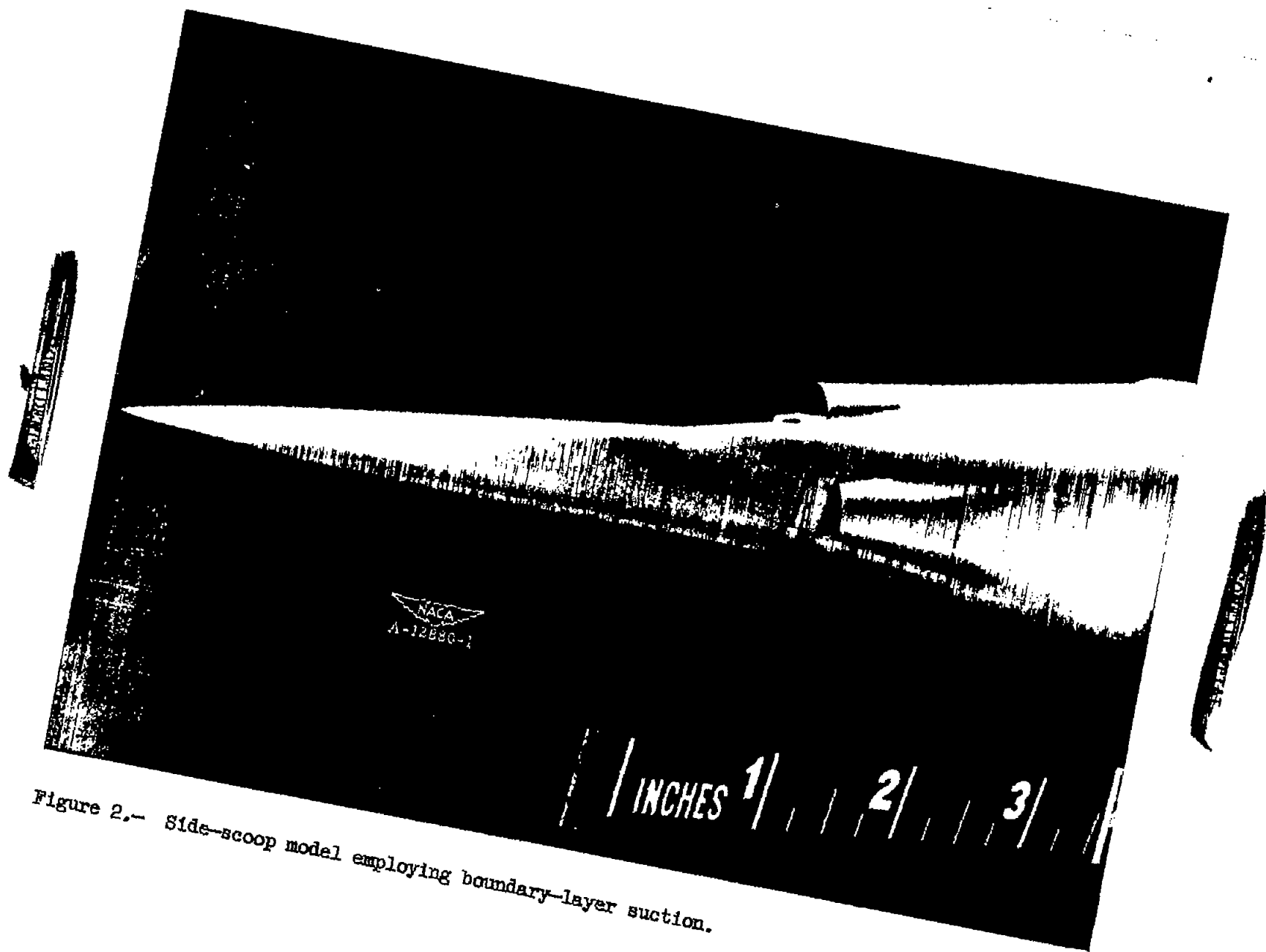


Figure 2.— Side-scoop model employing boundary-layer suction.



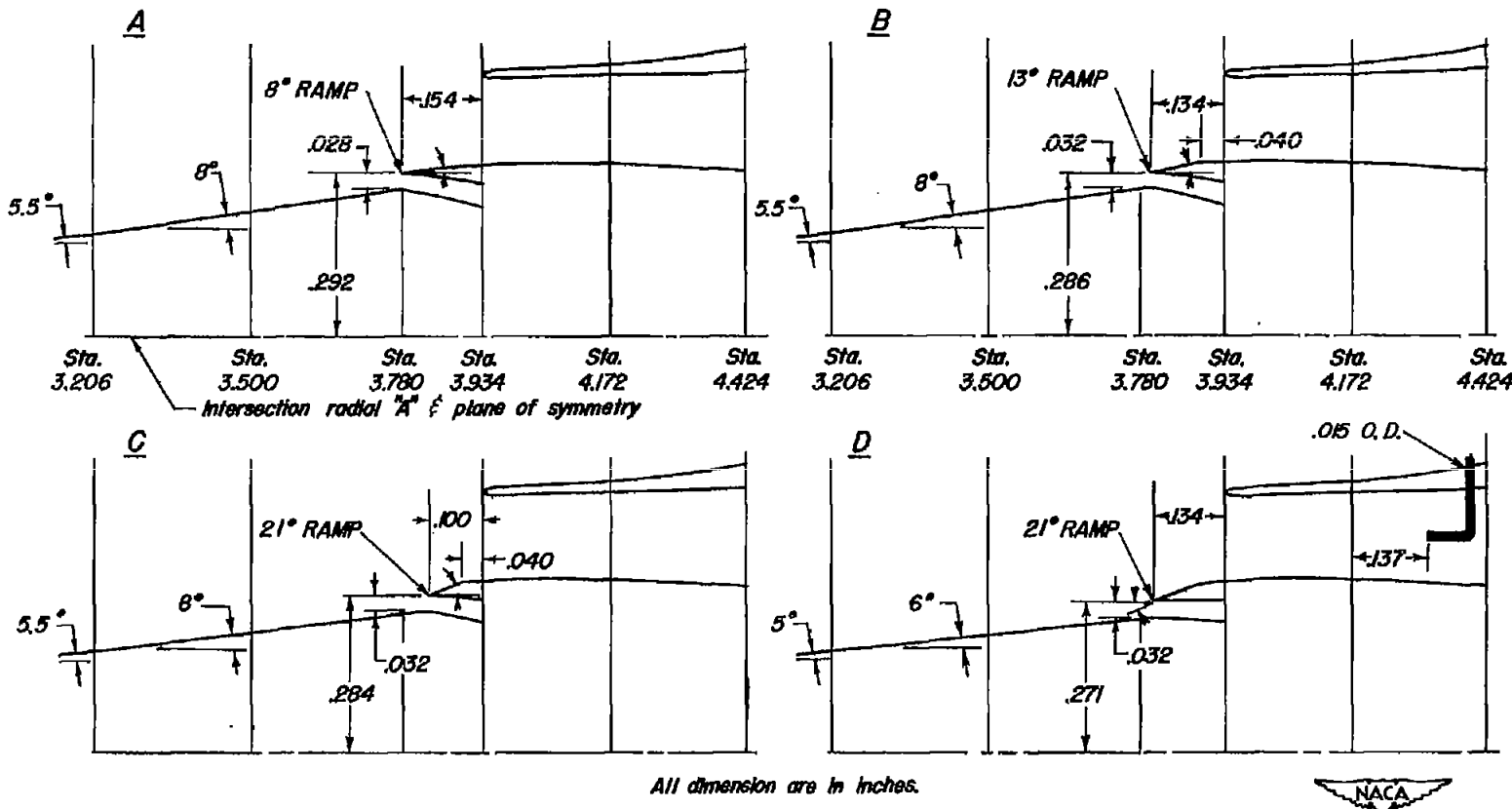
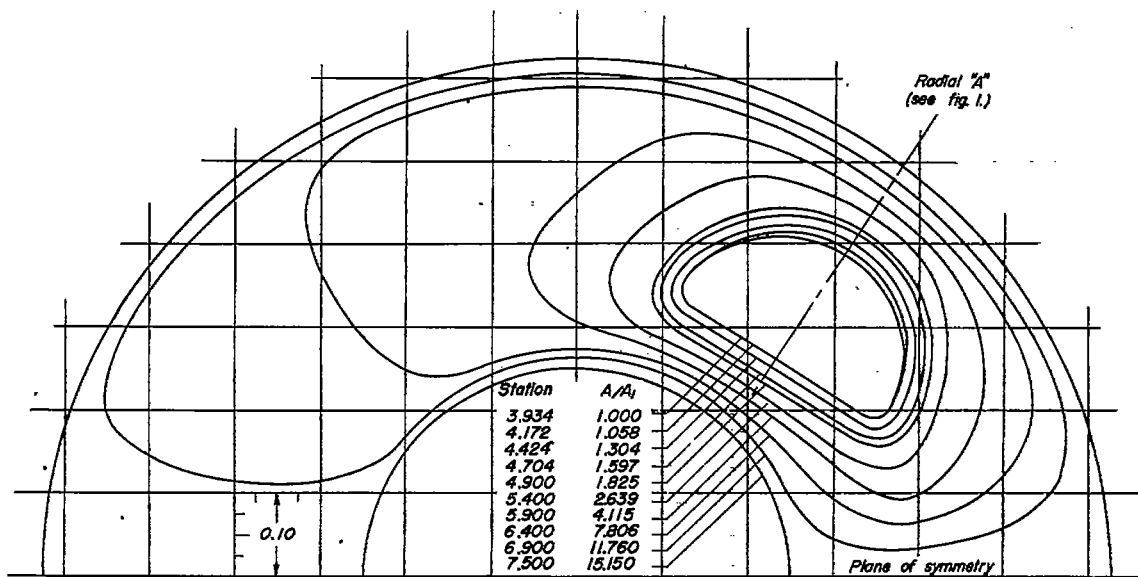


Figure 3.— Inlet configurations.



All dimension are in inches,

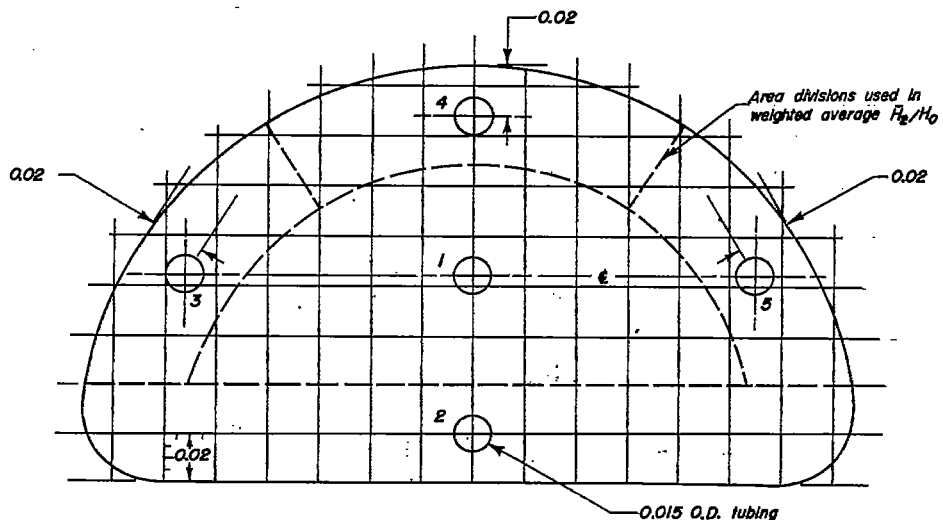


Figure 4. — Internal shape of main ducts and total-pressure-measurement locations at position 2.

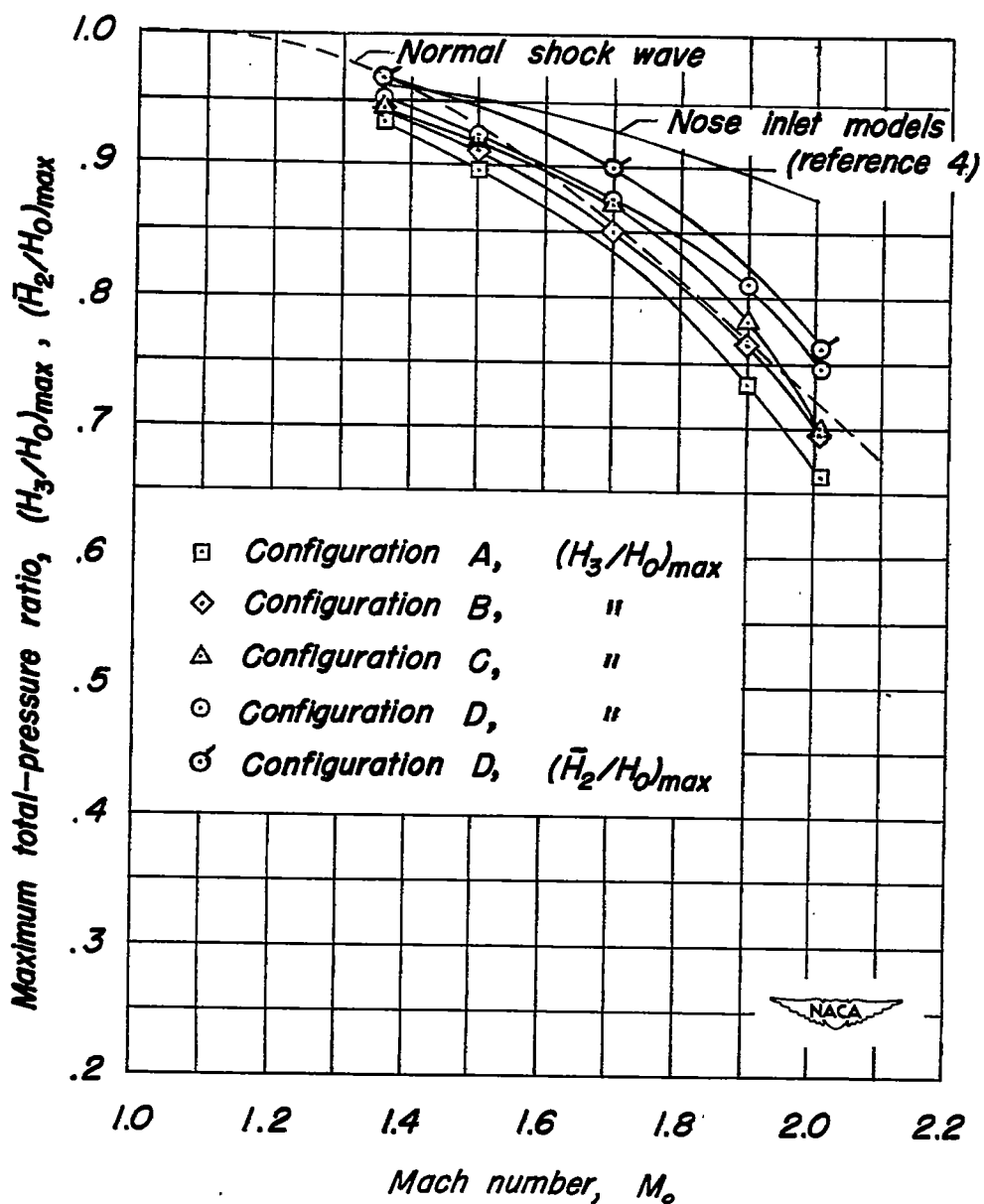
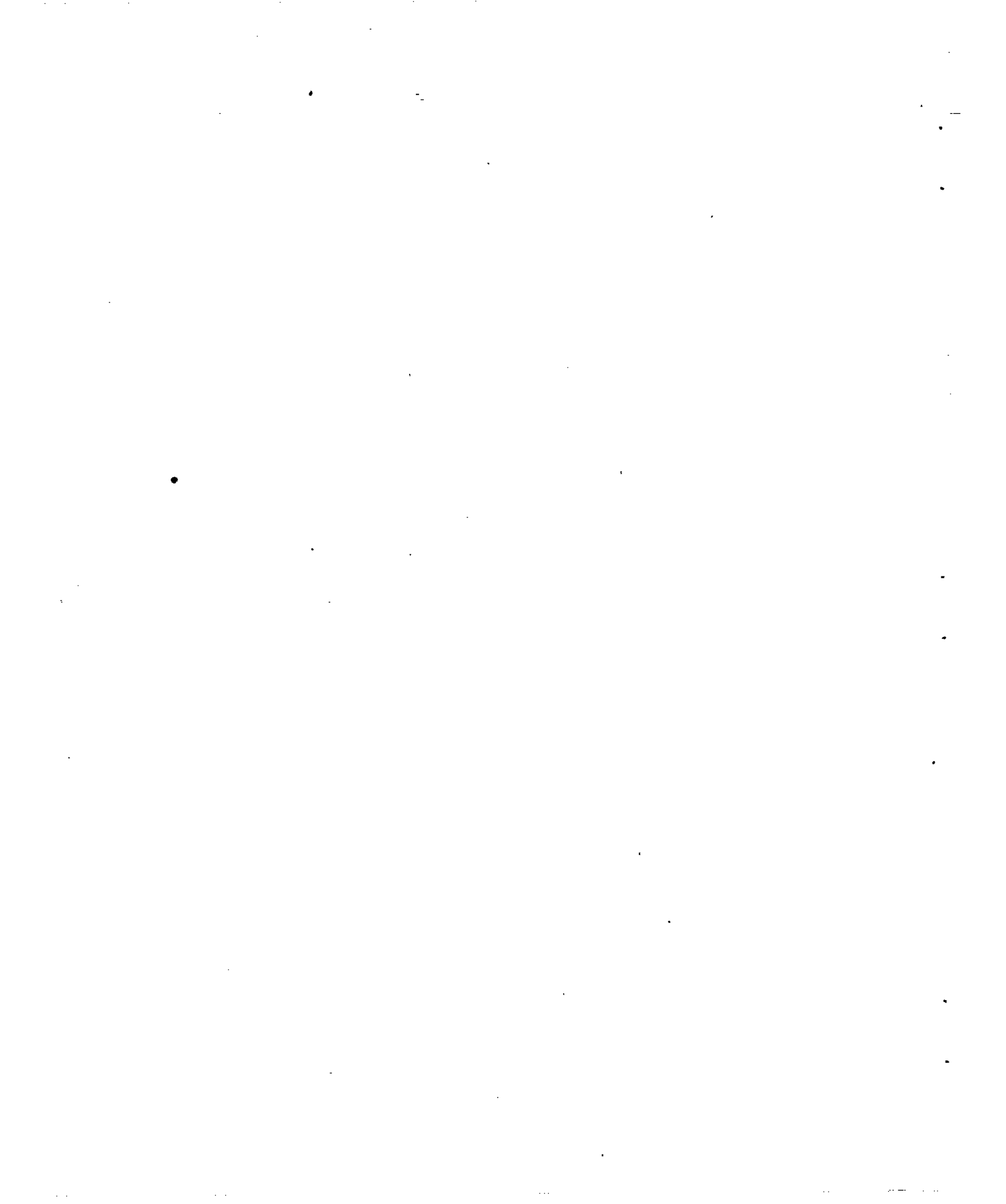


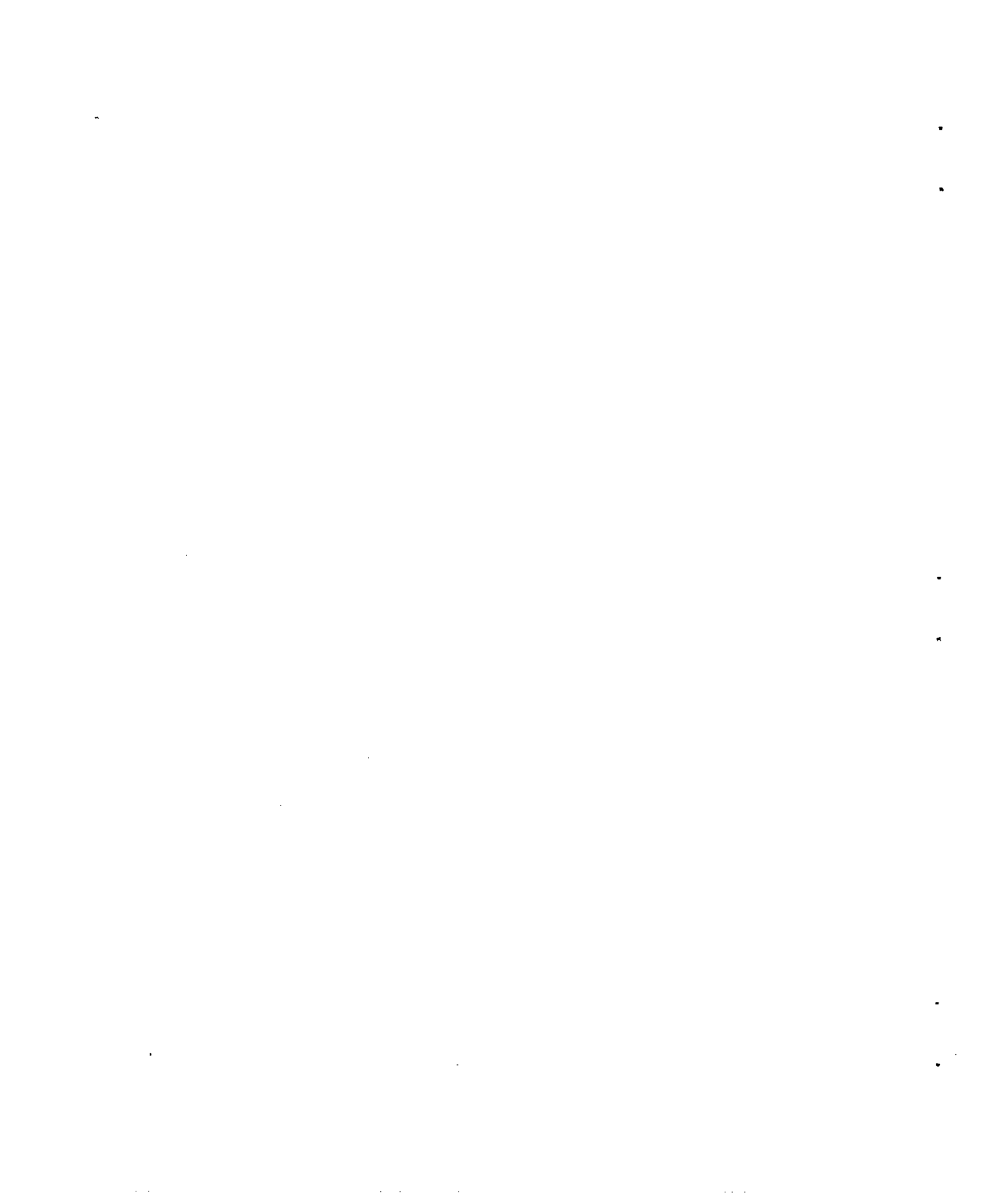
Figure 5.—Variation of maximum total-pressure ratio with free-stream Mach number;  $\alpha, 0^\circ$ ;  $m_4/m_0, \text{max.}$



(a)  $M_0$ , 1.36;  $m_1/m_0$ , 0.79.(b)  $M_0$ , 1.70;  $m_1/m_0$ , 1.10.(c)  $M_0$ , 2.01;  $m_1/m_0$ , 1.06.

NACA  
A-14359

Figure 6.— Schlieren photographs and schematic sketches of the flow about the model with inlet configuration D;  $\alpha$ ,  $0^\circ$ .



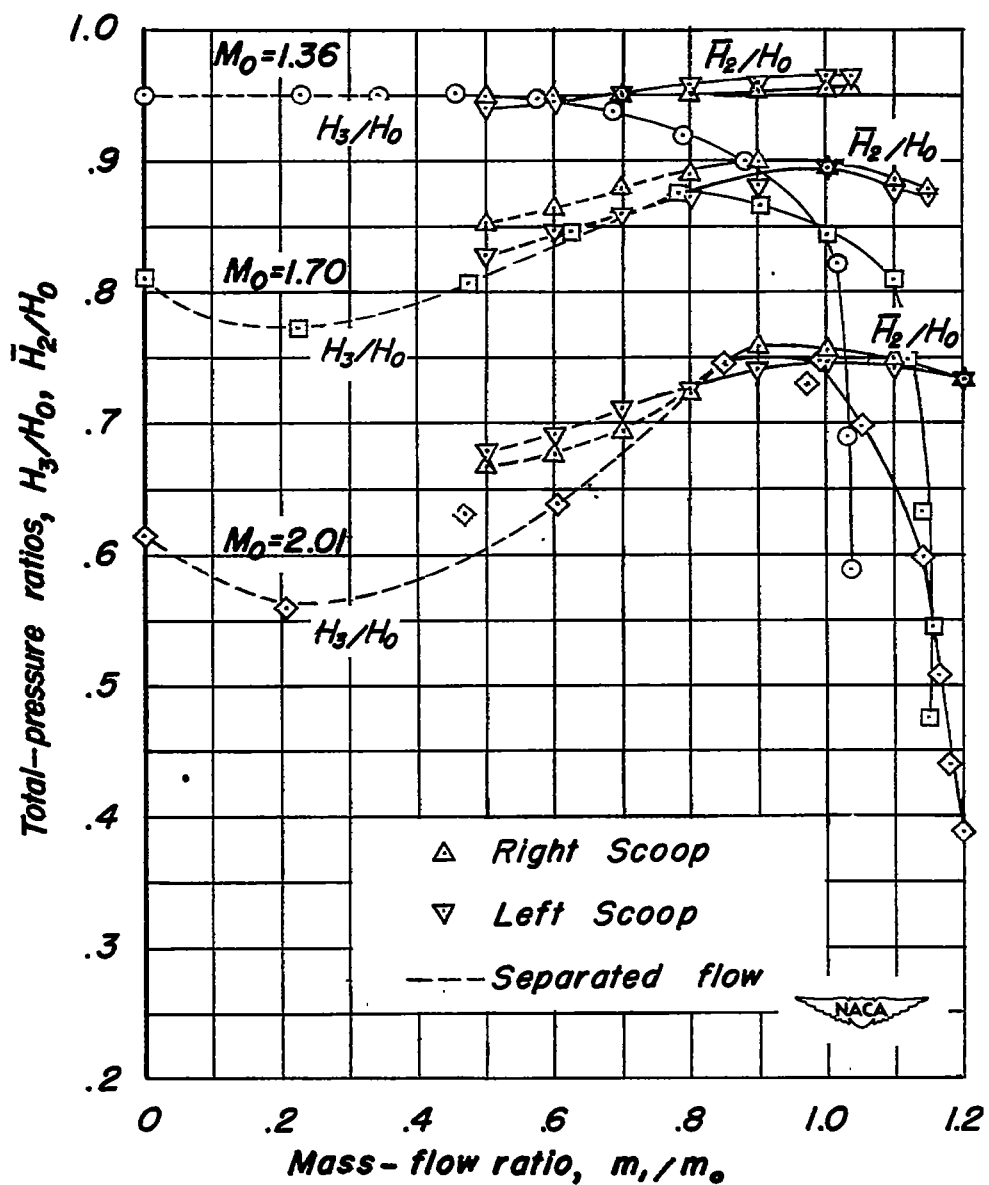


Figure 7.—Variation of total-pressure ratio with mass-flow ratio for configuration D;  $\alpha, 0^\circ$ ;  $m_4/m_0$ , max.

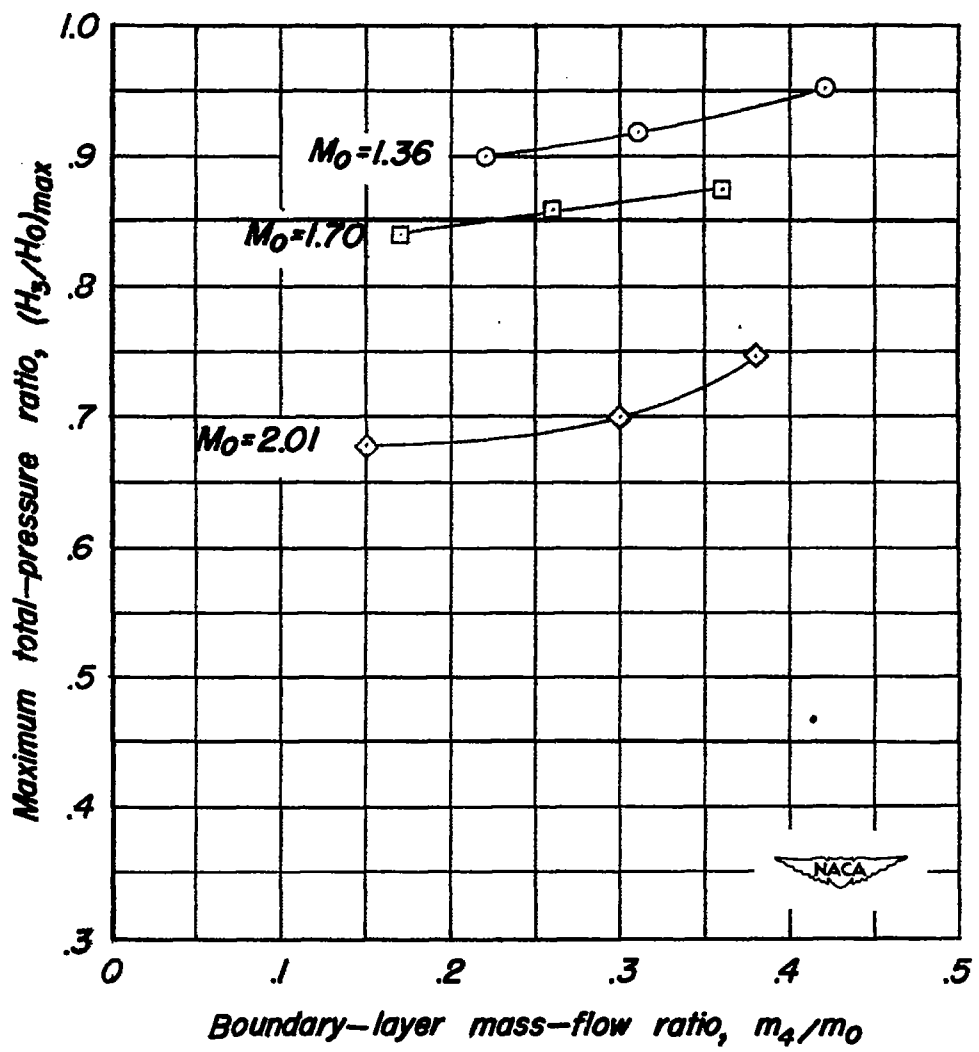


Figure 8.- Variation of maximum total-pressure ratio with mass flow in boundary-layer scoops of configuration D;  $\alpha$ ,  $0^\circ$ .

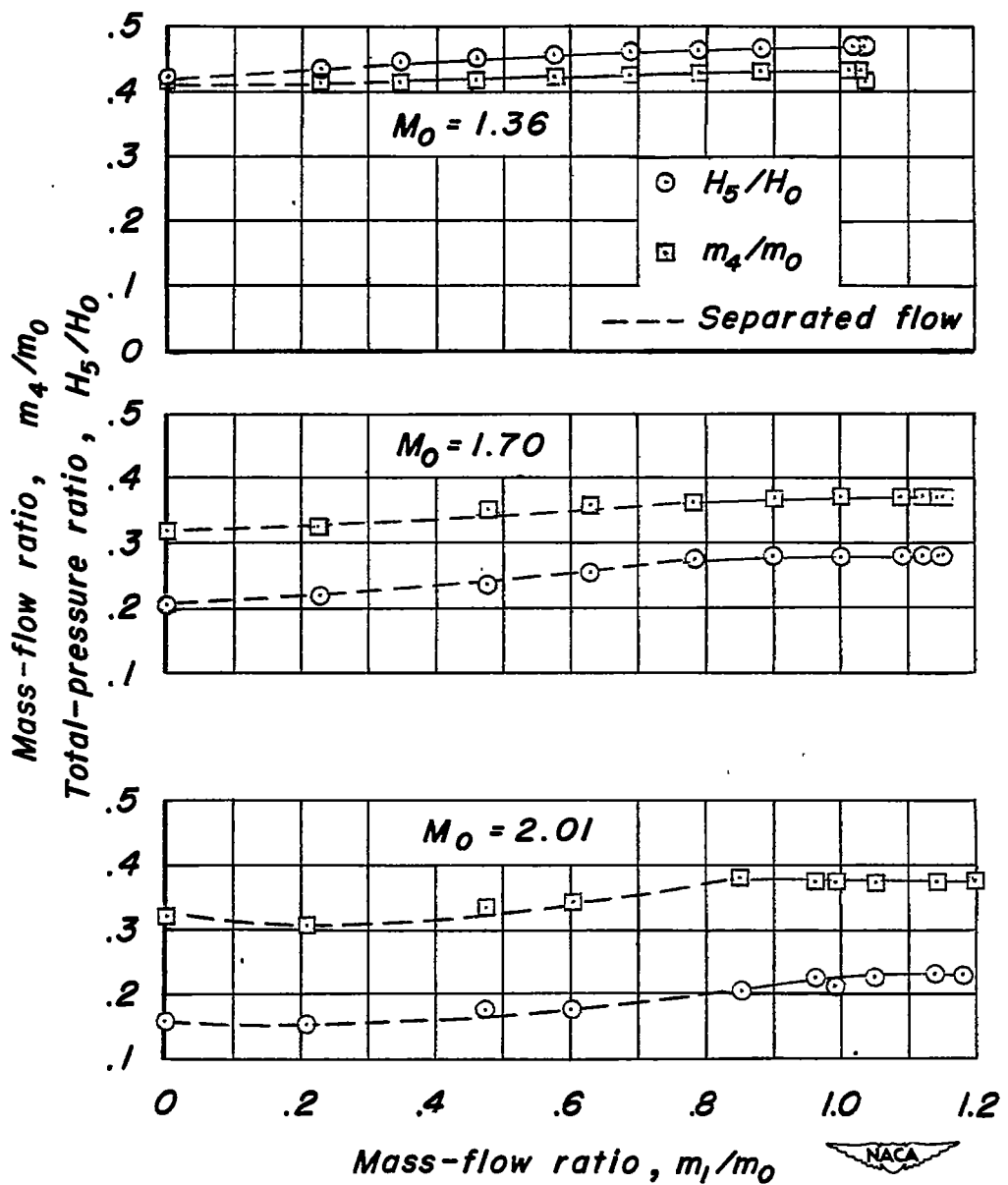


Figure 9.— Total-pressure ratio and mass-flow ratio in boundary-layer scoops at various mass flows in main scoops of configuration D;  $\alpha, 0^\circ$ .

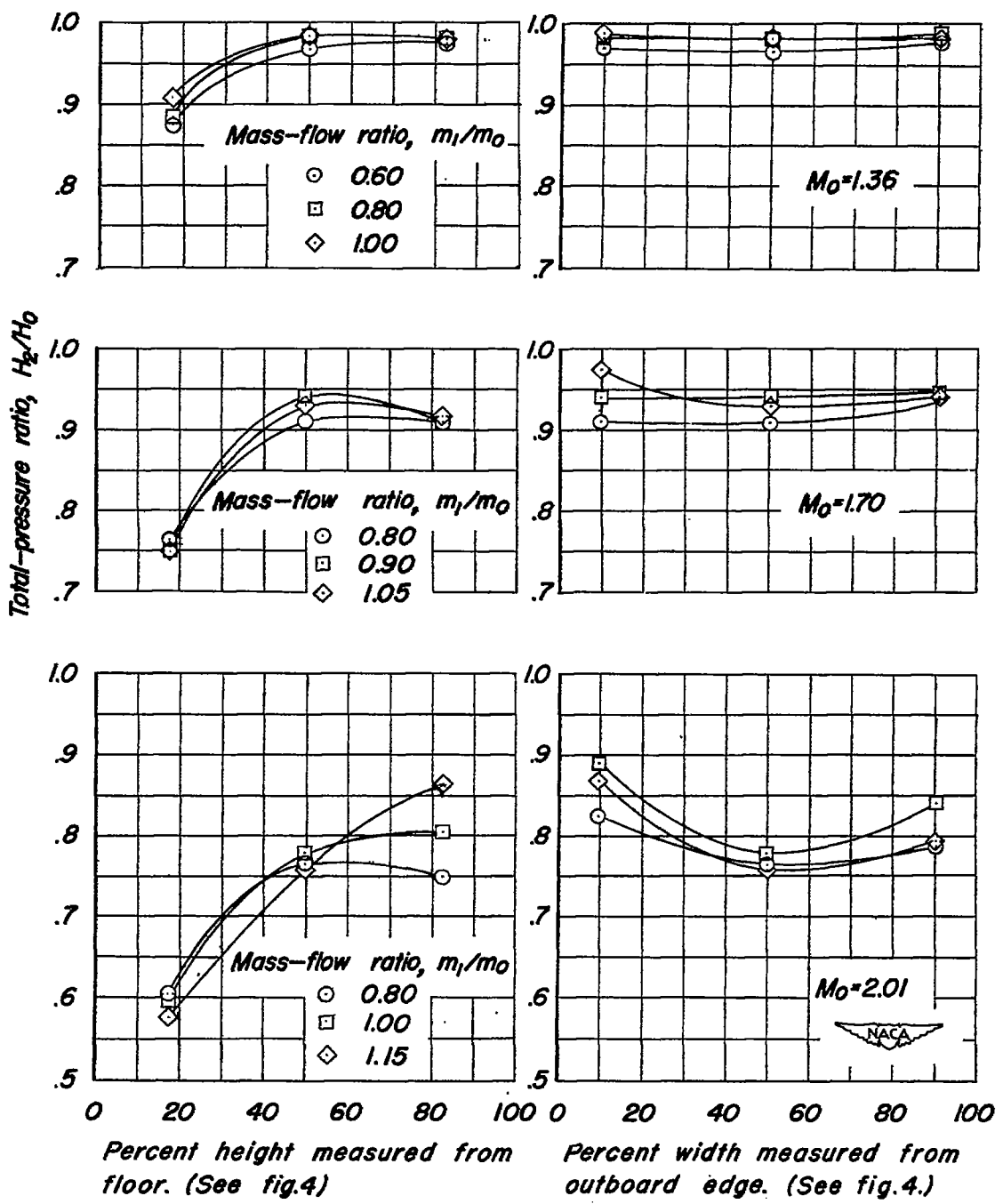
~~CONFIDENTIAL~~

Figure 10.— Total-pressure ratios measured at position 2 of configuration D;  
 $\alpha, 0^\circ$ .

~~CONFIDENTIAL~~

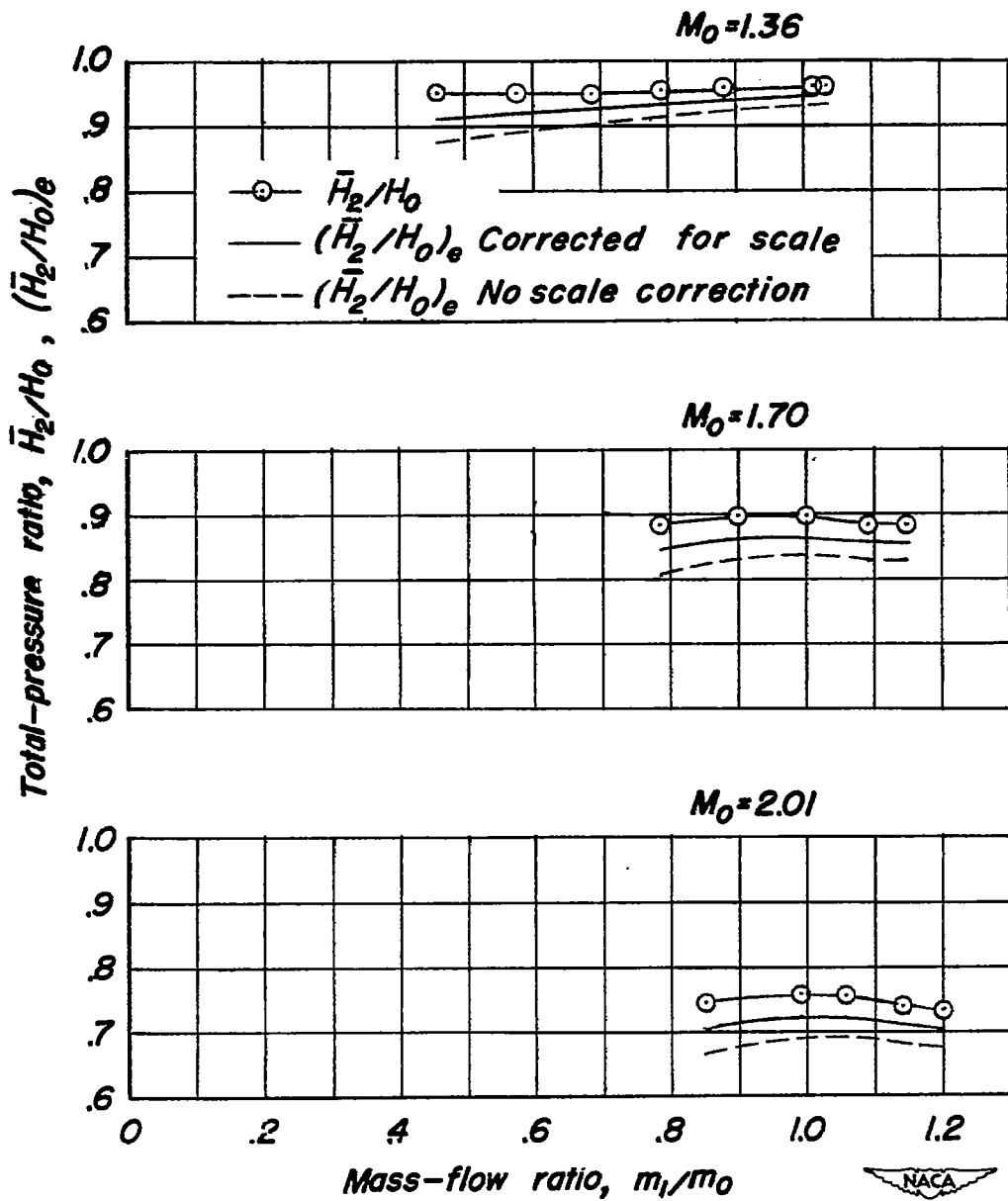


Figure 11.— Equivalent pressure recoveries at position 2 of configuration D;  $\alpha$ , 0°.

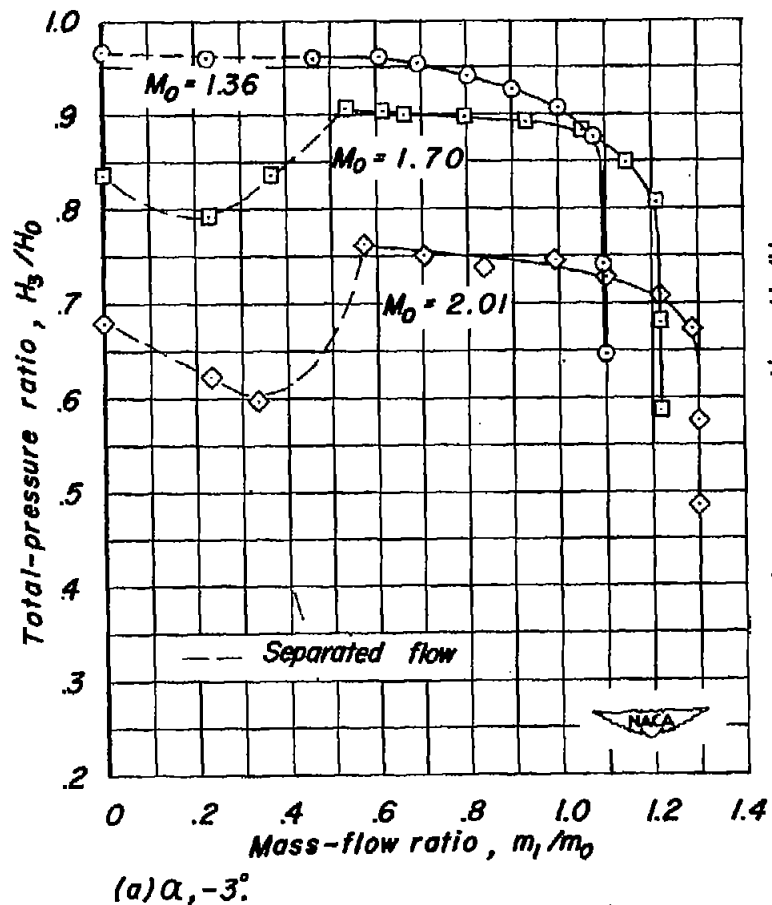
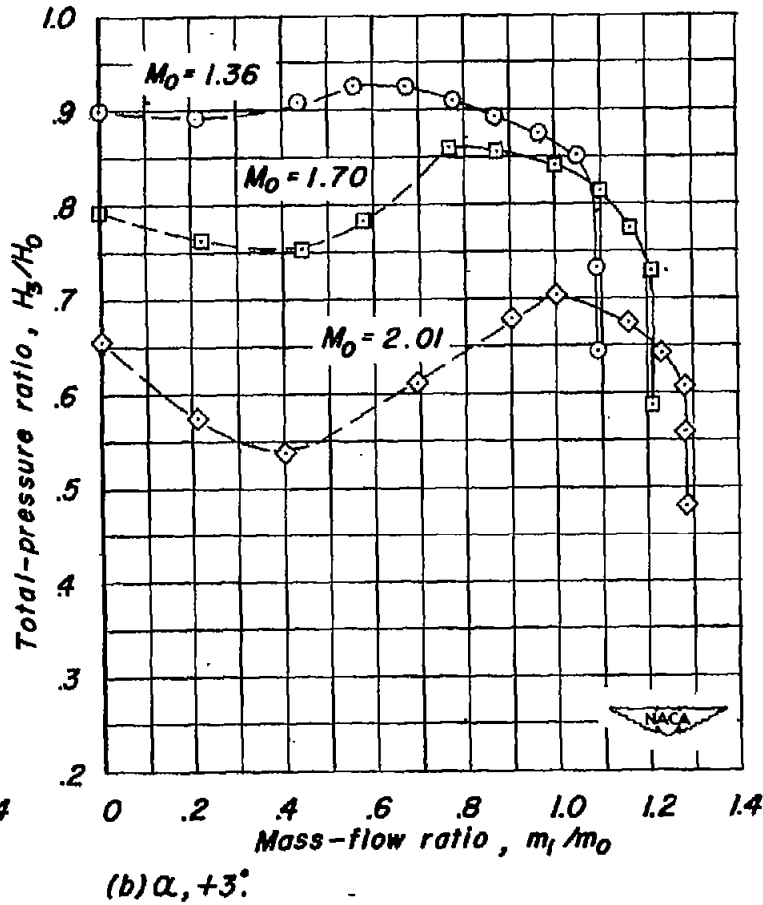
(a)  $\alpha, -3^\circ$ .(b)  $\alpha, +3^\circ$ .

Figure 12.—Variation of total-pressure ratio with mass-flow ratio for configuration D at angle of attack.

CONFIDENTIAL

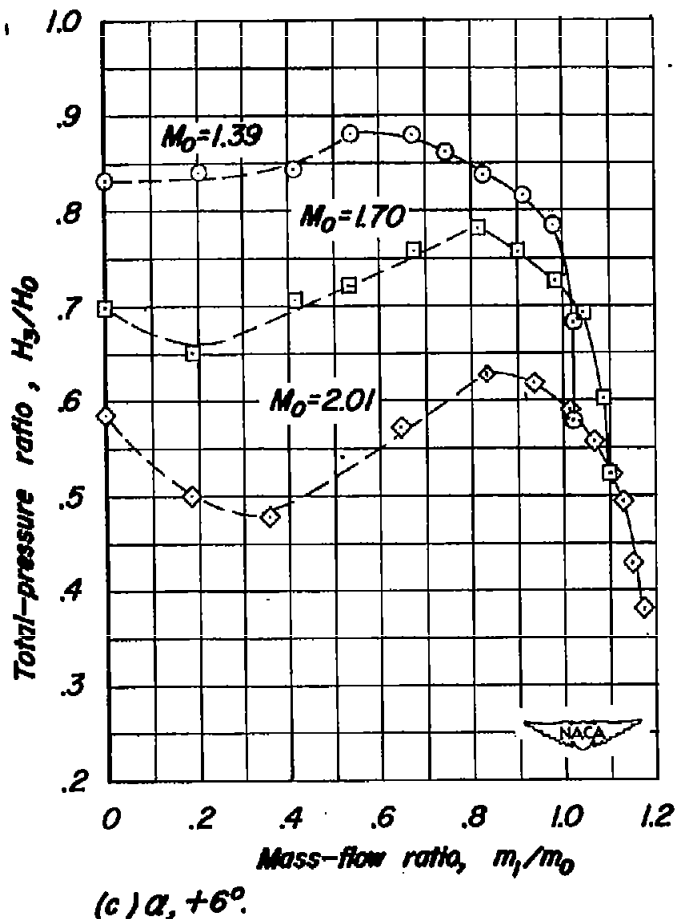
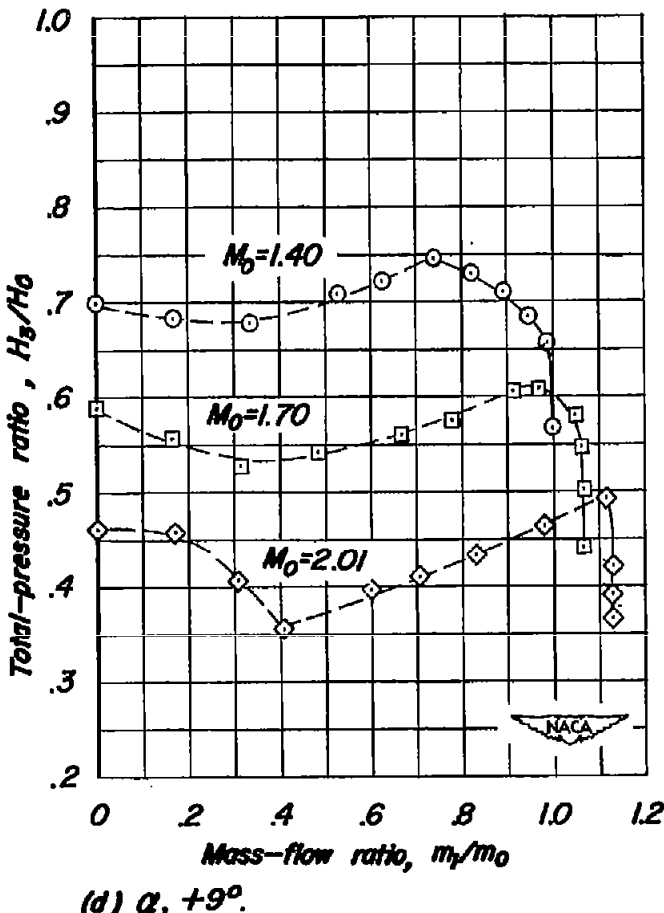
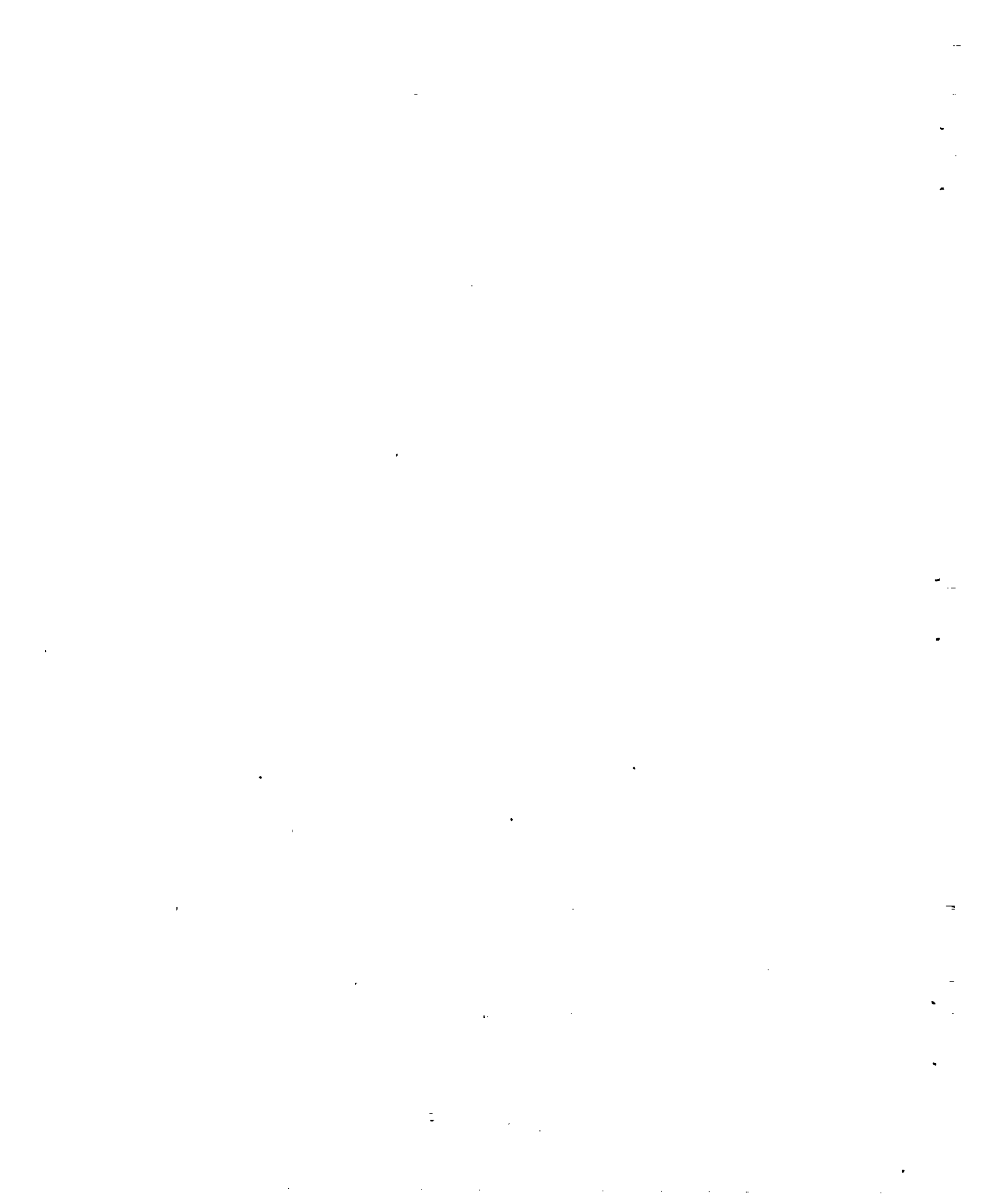
(c)  $\alpha, +6^\circ$ .(d)  $\alpha, +9^\circ$ .

Figure 12.—Concluded.



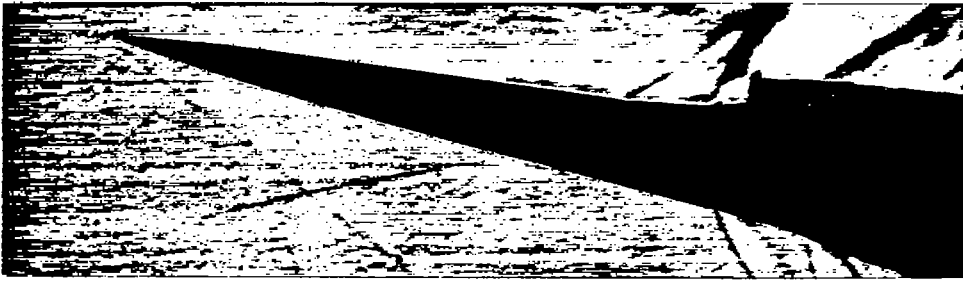
(a)  $\alpha, -3^\circ$ .(b)  $\alpha, 3^\circ$ .(c)  $\alpha, 6^\circ$ .(d)  $\alpha, 9^\circ$ . NACA  
A-13227

Figure 13.— Schlieren photographs of the flow about the model with inlet configuration A at  $M_0=1.70$  and various angles of attack.



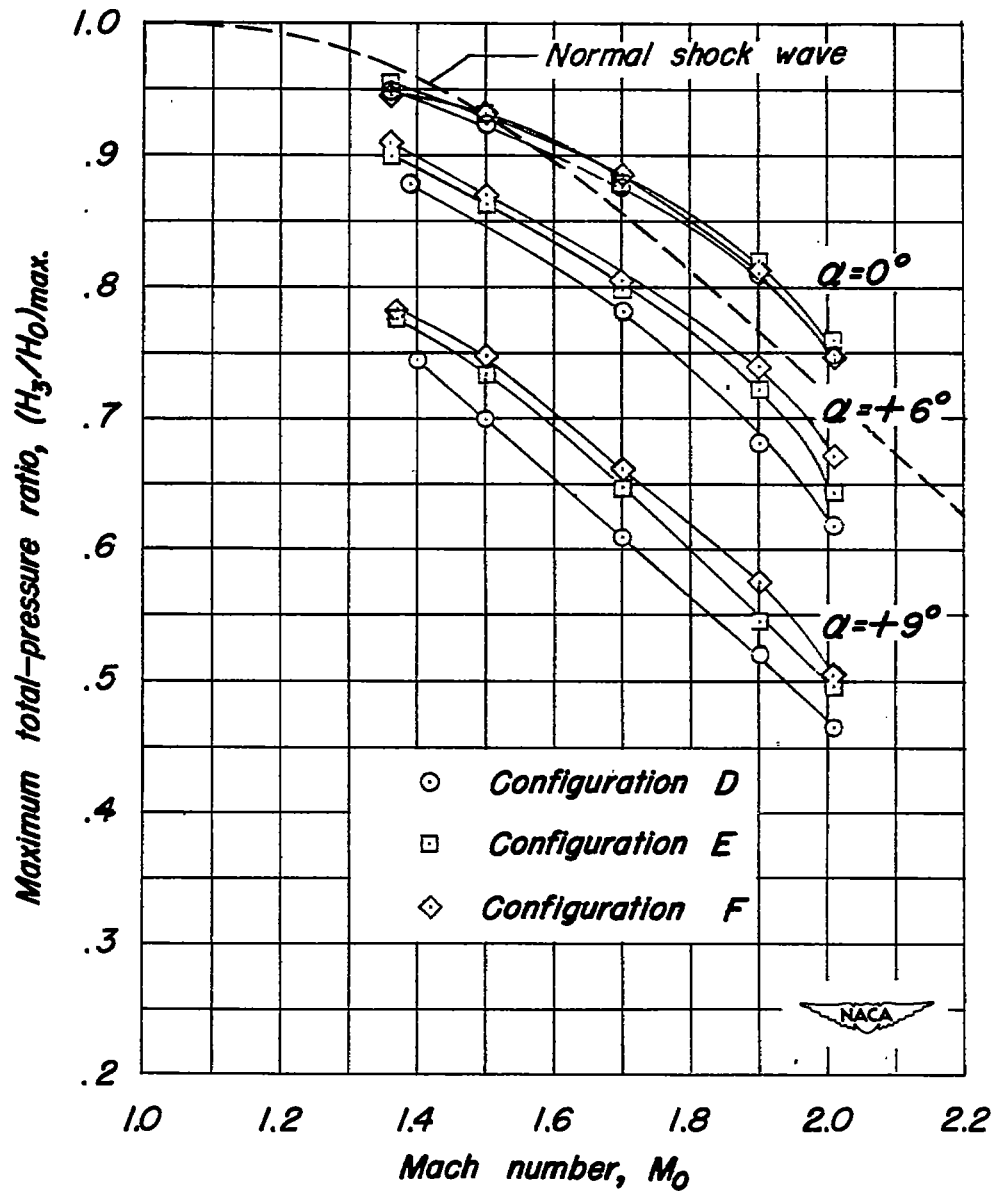


Figure 14. - Maximum total-pressure ratios at various Mach numbers and angles of attack.

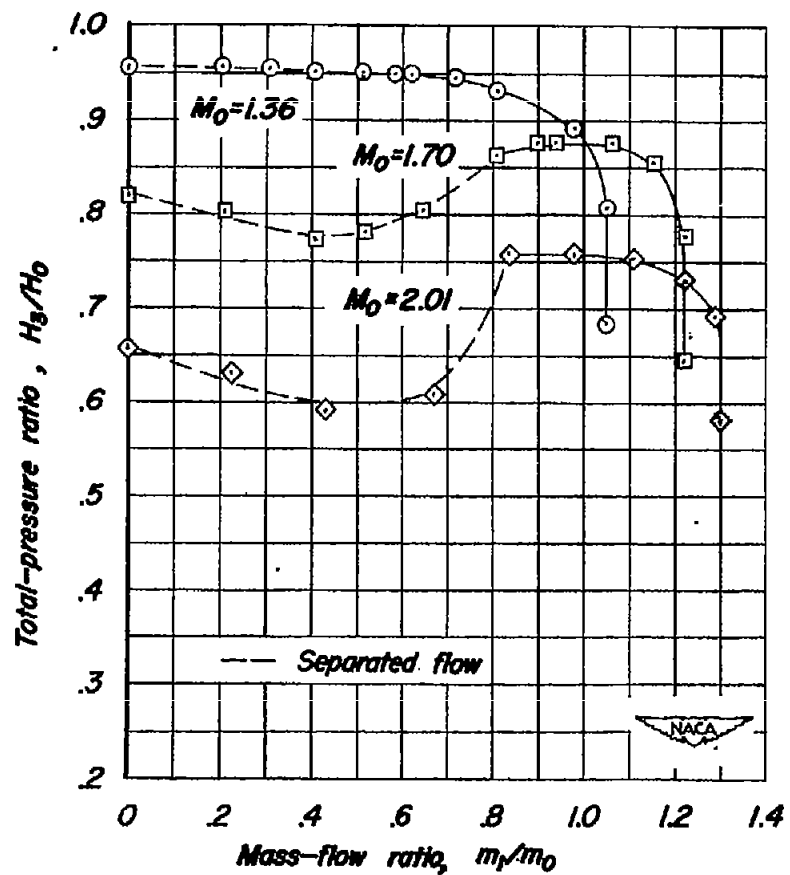
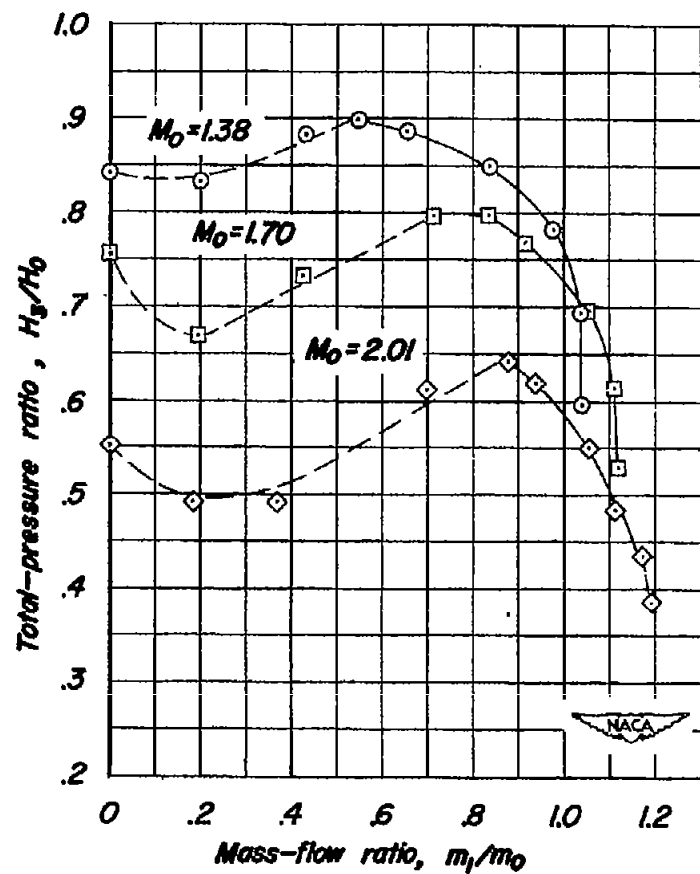
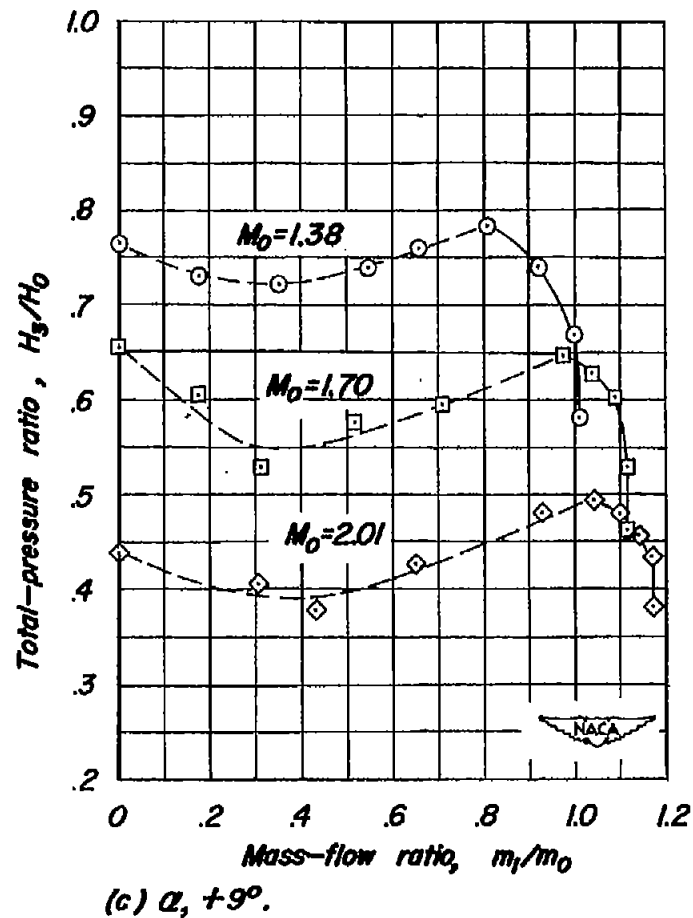
(a)  $\alpha, 0^\circ$ .

Figure 15.—Variation of total-pressure ratio with mass-flow ratio for configuration E at angle of attack.

(b)  $\alpha, +6^\circ$ .



(c)  $\alpha, +90^\circ$ .

Figure 15.—Concluded.

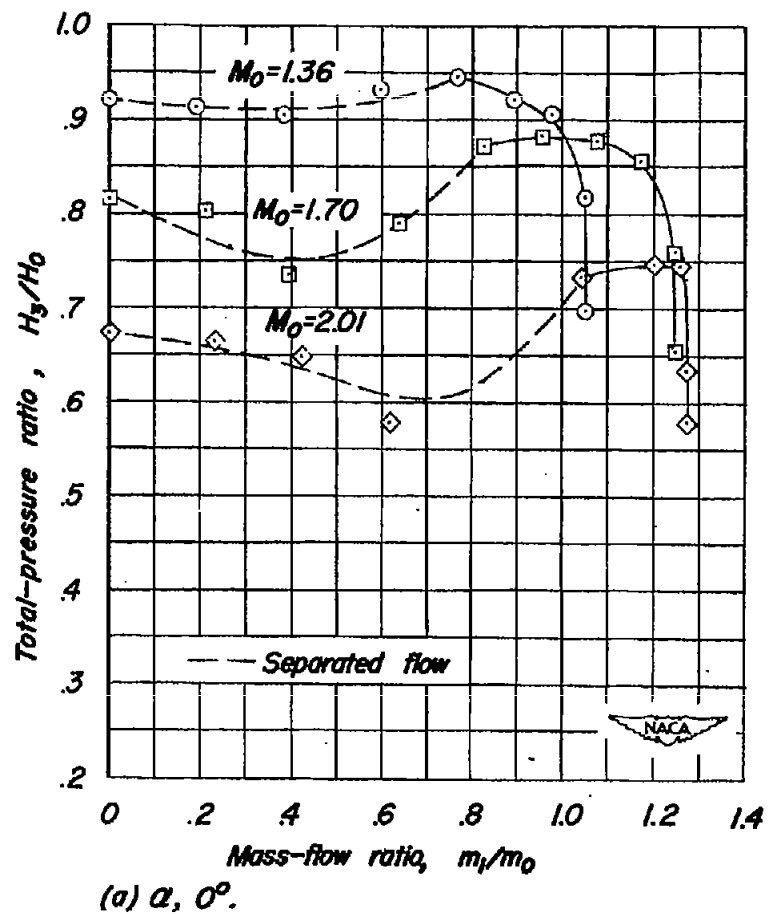
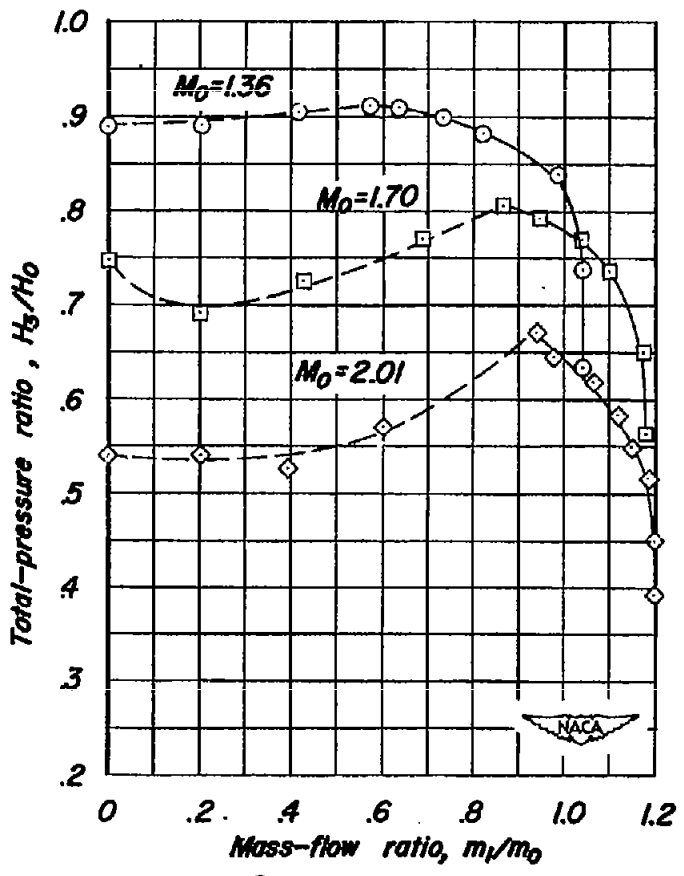
(a)  $\alpha, 0^\circ$ .

Figure 16.— Variation of total-pressure ratio with mass-flow ratio for configuration F at angle of attack.

(b)  $\alpha, +6^\circ$ .

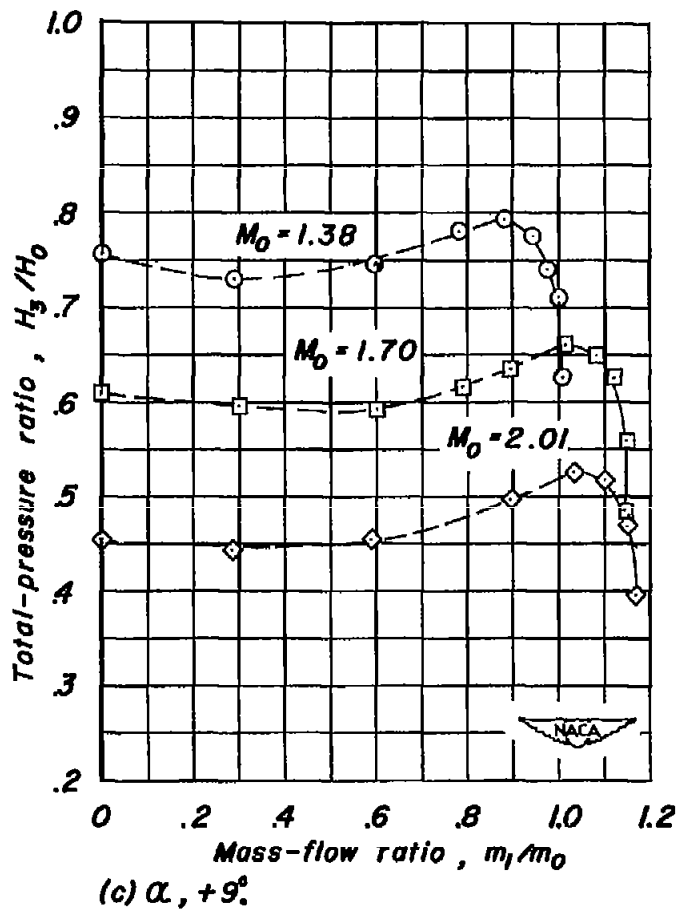


Figure 16. - Concluded.